## COMMUNICATION

# Ciliated micropillars for the microfluidic-based isolation of nanoscale lipid vesicles†

Zongxing Wang,[ab] Hung-jen Wu,[a] Daniel Fine,[a] Jeffrey Schmulen,[a] Ye Hu,[a] Biana Godin,[a] John X. J. Zhang*[b] and Xuewu Liu*[a]

**We fabricated a microfluidic device consisting of ciliated micropillars, forming a porous silicon nanowire-on-micropillar structure. We demonstrated that the prototype device can preferentially trap exosome-like lipid vesicles, while simultaneously filtering out proteins and cell debris. Trapped lipid vesicles can be recovered intact by dissolving the porous nanowires in PBS buffer.**

Exosomes are lipid membrane vesicles, 40–100 nm in diameter, that are shed from the majority of viable cells into the extracellular space, and then excreted in a range of bodily fluids, including blood, urine, and saliva, as well as synovial and amniotic fluid.[1–6] Exosomes contain a variety of high-purity molecular constituents from their cell of origin, such as lipids, cell specific proteins, and RNA (mRNA and miRNA), thus constituting an informative resource for studying important molecular events in disease progression.[7] The analysis of the contents of exosomes may therefore represent a potentially powerful diagnostic tool for the early detection of various malignancies, as demonstrated previously for diabetes as well as lung, prostate, and colorectal cancer.[8,9] Isolating high purity exosomes to avoid contamination, such as from serum proteins, would help to acquire more accurate biological information on the cells/tissues they originated from. For molecular analysis, it is not necessary to recover intact isolated exosomes, as, instead, one can lyse the isolated exosomes and analyze their molecular constituents. However, intact exosomes are required for specific applications such as delivery carriers of biologically active substances. Moreover, the recovery of intact exosomes will allow us to distinguish the cellular origins of exosomes, and evaluate the morphological features of these vesicles. Intact exosomes can be used to specifically target recipient cells to deliver proteins, lipids and nucleic acid cargo,

to participate in intercellular communication, and to trigger signalling events.[10,11] Exosomes can also be facilitators of the immune response for antigen presentation,[12] act as immune suppressors in cancer,[13] and become morphogen transporters in cell development and differentiation.[14] Exosomes have also been utilized as drug carriers, able to efficiently cross the blood–brain-barrier to knock down a therapeutic target in an Alzheimer's mouse model,[15] and as a stem cell alternative in stem cell-based therapies for cardiovascular diseases.[16–18]

For both diagnostic and therapeutic applications, an efficient separation technique is required to isolate exosomes from raw biological fluids that also contain high quantities of proteins, protein aggregates, and cell debris with similar physical characteristics. The conventional differential centrifugation procedure,[19] which involves a series of centrifugation, filtration, and ultracentrifugation steps, suffers from inconsistent exosome recovery rates (5–23%) and contamination from co-sedimentation of protein aggregates.[20] Several immunoisolation assays based on either magnetic beads or microfluidic devices have also been demonstrated using antibody-based affinity capture for rapid exosome isolation.[7,21] These methods would require specific exosomal surface proteins or antibodies to be available for discrimination between the exosomes of interest and other species in the fluids.[7,22,23]

In this paper, we present a microfluidic device consisting of ciliated micropillars capable of simultaneous multi-scale filtration. The cilia consist of porous silicon nanowires that are electrolessly etched on the micropillar sidewalls using electrodeposited silver nanoparticle catalysts. Using liposomes of known size as model vesicles, we have demonstrated that the ciliated micropillars preferentially trap exosome-like lipid vesicles while allowing smaller proteins and larger nanoparticles with the size of cellular debris to pass by unhindered. Moreover, the captured lipid vesicles can be released by dissolving the porous silicon nanowires in PBS buffer, thus allowing for their intact and highly purified recovery.

### Ciliated nanowire-on-micropillar structure

We fabricated our novel multidimensional hierarchical structure with a combination of silicon microfabrication processes, electro-

[a]Department of Nanomedicine, The Methodist Hospital Research Institute, Houston, Texas, USA. E-mail: xliu@tmhs.org

[b]Department of Biomedical Engineering, University of Texas at Austin, Austin, Texas, USA. E-mail: John.Zhang@engr.utexas.edu

† Electronic supplementary information (ESI) available: Materials and methods used in the paper are described in the supporting information. See DOI: 10.1039/c3lc41343h
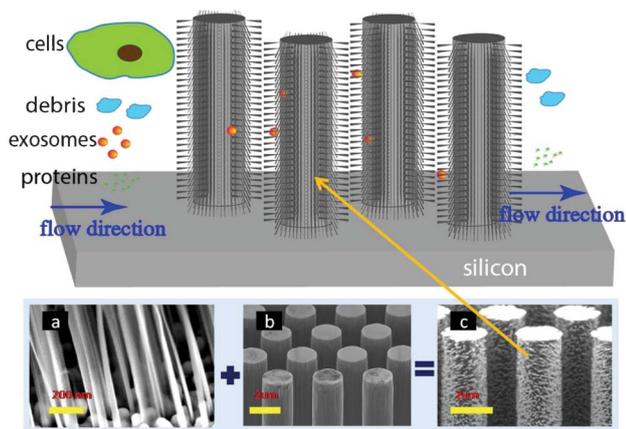
**Fig. 1** A schematic of the ciliated micropillar array for exosome isolation. The cells are depleted before entering the micropillar region, while cellular debris as well as proteins and other small objects flow through, bypassing the micropillars. Exosomes are highly enriched by trapping within the nanowires. Insert (a): representative porous silicon nanowire forest. Insert (b): micropillars. Insert (c): representative ciliated micropillars.



**Fig. 2** SEM images of the ciliated micropillar fabrication stages. (a) Uniform silver deposition is achieved using the pulse reverse plating method. (b) A close-up view of (a). (c) Porous silicon nanowires are formed on the sidewalls of the micropillars using an electroless etch. (d) A close-up view of (c). When using electroless silver deposition, most of the deposition occurs near the bottoms of the micropillars for high resistivity wafers (e) and near the tips for low resistivity wafers (f). All scale bars are 2 μm.

plating, and electroless metal-assisted nanowire etching techniques. We then assembled the ciliated micropillar microfluidic prototype with a poly(dimethylsilozane) (PDMS) cap for the rapid and efficient isolation of exosome-like nanoscale vesicles. As illustrated in Fig. 1, porous silicon nanowires were etched into the sidewalls of the micropillars by metal assisted etching.[24] The inter-nanowire spacing in the nanowire forest can be tuned within a range of 30–200 nm (Fig. 1 inset a), thus creating a high density of interstitial sites capable of physically trapping exosome-like nanoparticles. In addition to providing walls for anchoring the nanowires, the micropillars (Fig. 1 inset b) also filter larger sample components, including cells, and function as the structural supports for the microfludic channel. This nanowire-on-micropillar hierarchical structure (Fig. 1 inset c) therefore interacts with biological fluid samples at multiple length scales (Fig. 1): (1) cells are depleted from the micropillar array owing to the sub-micron inter-pillar spacing; (2) submicron cellular debris can enter the micropillar area but is excluded by the nanowire forest (30–200 nm inter-nanowire spacing); (3) proteins and other molecules pass through the spacing in the nanowire forest without being captured; (4) objects with sizes in the range of exosomes are trapped in the interstitial sites within the nanowire forest; and (5) the 6–10 nm pores of the porous silicon nanowires can be pre-loaded with multiple components, such as antibodies or biomolecules, to further enhance selectivity and functionality. The porous silicon nanowires can then be dissolved in PBS buffer to recover the intact and purified trapped nanoparticles.

**Fabrication of the ciliated micropillars**

Arrays of 2.6 μm circles were patterned on a silicon wafer by photolithography, followed by a deep silicon etch (DSE) using an Inductively Coupled Plasma (ICP) Reactive Ion Etcher (RIE, Plasmatherm Versaline), to form arrays of 22 μm tall micropillars. Silver nanoparticles were deposited onto the micropillar side-walls using a pulse reverse plating method in a AgNO₃ solution and then etched into the complete circumference of the micropillar
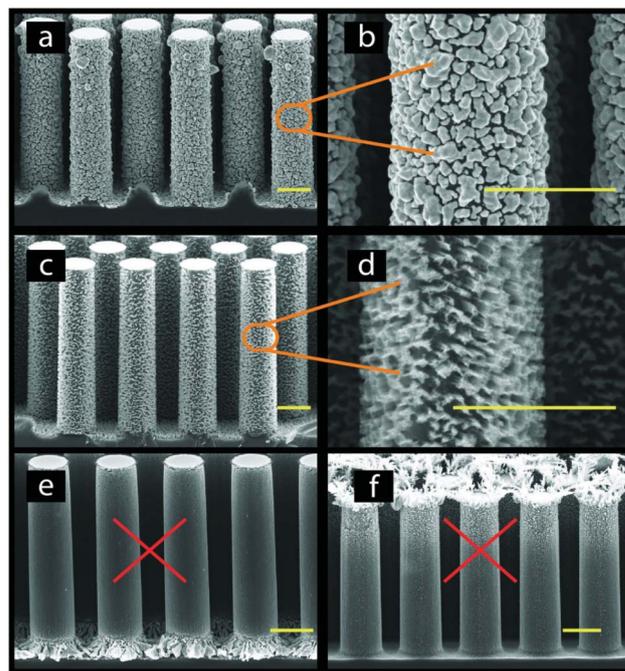
side-walls by metal assisted chemical etching (previously described in ref. 24) to a depth of 400 nm. The top surface of the micropillars were protected by a silicon nitride layer for subsequent PDMS capping. This nanowire-on-micropillar structure was capped with PDMS to create the final filter prototype.

The distribution of the nanowires, and thus the interstitial spacing that leads to enhanced exosome trapping efficiency, is controlled by the silver nanopatterning process. Standard electro-less silver deposition is governed by the kinetics of the electrochemical reaction and reactant diffusivity, as well as the properties of the reactants and silicon substrates onto which the silver is deposited. In the case of tall micropillars with surface irregularities, this diffusion and substrate surface property dependence can result in a non-uniform silver accumulation along the vertical direction of the micropillars,[25] as shown in Fig. 2e and f. To achieve a uniform silver nanoparticle deposition on the micropillar surface, a pulse reverse plating method was adapted (see Reverse pulse silver deposition on the sidewalls of micropillars; Fig. S1, ESI†).[26] Depending on the feature size of the micropillar structure, the pulse cycles were tuned accordingly to optimize the silver pattern (Fig. 2a and b). Uniform nanowire arrays were then subsequently etched onto the micropillar surface from the optimized silver pattern as shown in Fig. 2c and d.

**Design of the ciliated micropillar based microfluidic prototype**

Our proof-of-concept microfluidic-based prototype consists of a 4 mm long concentric radial-flow fluidic channel (total area is 235
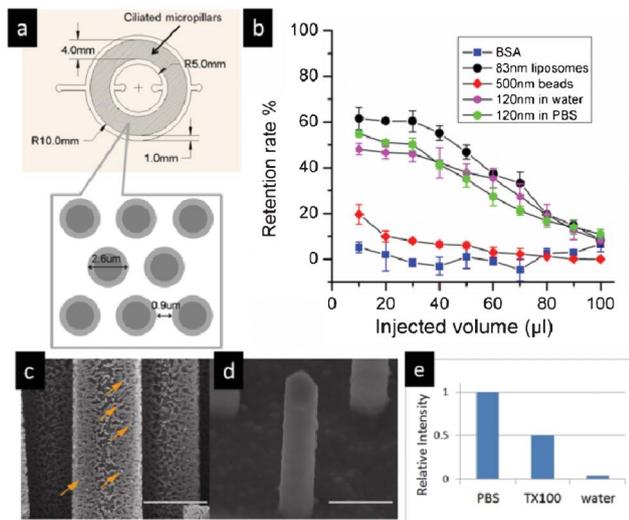
**Fig. 3** The ciliated micropillar microfluidic filtering of liposomes. (a) Schematic of the microfluidic prototype device. (b) Percentage of retained nanoparticles and proteins *versus* the injected volume for FITC-BSA, 83 nm liposomes, 120 nm liposomes and 500 nm polystyrene beads. (c) SEM image of QDs trapped on ciliated micropillars, as indicated by the arrows. (d) SEM image of the remaining micropillars after soaking in PBS buffer to remove the nanowires. (e) The relative recovery yields from three different methods: soaking in PBS, washing with TX100 solution, and flushing with water. All scale bars are 2 μm.

mm$^2$), containing hexagonally packed ciliated micropillars, 2.6 μm in diameter, 22 μm tall, and spaced at 900 nm apart, that is capped with PDMS and capable of capturing ~100 μg of lipid nanoparticles (Fig. 3a). 400 nm long porous silicon nanowires coat the sidewalls of the micropillars. The channel design was developed based on the Comsol simulation results, indicating that a radial-flow fluidic channel would minimize the trans-channel pressure drop as compared to a straight fluidic channel (see Flow resistance in microfluidic channels with micropillars; Fig. S2, ESI†). Furthermore, several key parameters of the ciliated micropillars were optimized for efficient exosome isolation: the height and density of the micropillars, as well as the morphology of the nanowires. Higher micropillar densities and longer nanowires provide more binding sites for exosomes, but will lead to higher hydrodynamic resistance within the microfluidic network and may increase the risk of clogging. The 900 nm spacing between micropillars was selected to deplete the micron size cells in biological fluids. A circular inlet and outlet were also connected to the micropillar area for sample introduction and extraction. The fabrication process flow and processing details of the prototype devices can be found in the supporting information (see Fabrication of ciliated micropillar microfluidic devices; Fig. S3, ESI†).

### Prototype validation

Sample solutions containing fluorescently labeled 83 nm liposomes, 120 nm liposomes, 500 nm polystyrene nanoparticles, and 7 nm fluorescein isothiocyanate labelled bovine serum albumin (FITC-BSA)[27] were used to verify the functionality of our microfluidic-based prototype (see ESI,† Fig. S3, for the experimental setup). A high precision syringe pump (PHD Ultra Syringe

Pump, Harvard Apparatus) was connected to the inlet through the PDMS cap using 1 mm O.D. tubing and used to inject the samples. The samples were then extracted at the outlet, also through 1 mm O.D. tubing. The fluorescent intensities of the injected and collected samples were analyzed using a plate reader (Synergy H4 Hybrid) to determine the concentrations of liposomes, nanoparticles, and protein in each. The difference in concentration between the injected and collected samples was then used to calculate the quantity of liposomes, nanoparticles, and protein that were retained by the microfluidic-based ciliated micropillar prototype. The quantity of the retained liposomes, nanoparticles, and FITC-BSA as a percentage of the injected amount is plotted *versus* the injected sample volume in Fig. 3b. The 500 nm polystyrene nanoparticles that simulate possible cellular debris show very little retention, while FITC-BSA that represents an abundant protein constituent *in vivo* shows almost no retention. As expected, the microfluidic-based ciliated micropillar prototype demonstrates its highest retention for the 83 nm liposomes at nearly 60% for an initial amount of up to 30 μL of sample injected. The 120 nm liposomes show a similar trend to the 83 nm liposomes, but the overall retention is decreased by about 15%. We also compared the retention of the 120 nm liposomes in both water and PBS, and found no significant difference between water and the PBS conditions. From these data, we can conclude that our device provides larger amounts of binding sites and niches for exosome-sized vesicles, leading to a substantially enhanced quantity of retention as compared to both larger (500 nm nanoparticles) and smaller (proteins) sized analytes.

### Dissolving the nanowires to release the captured liposomes

The particle retention by the nanowires was also directly visualized using quantum dots (QD, Qtracker 655, Invitrogen). The QDs used here are ~40 nm in diameter and carry no net surface charge in PBS buffer. After the QD solution was injected into the prototype and flushed, the QDs trapped by the nanowires were observed using SEM (Fig. 3c). In contrast, the ciliated micropillars soaked in PBS overnight were unable to retain QDs as a result of the chemical etching of the nanowire surface coating by the PBS buffer, leaving only the thinned micropillars behind (see Fig. 3d).

We hypothesized that this degradation of the porous silicon nanowire coating could be used to recover the trapped 83 nm liposomes. To test this, liposome solutions were injected into the microfluidic-based prototype for a total volume of 100 μL, after which the fluidic channel was flushed with 1 mL of water. Liposome recovery from the microfluidic-based ciliated micropillar prototypes was then measured under three conditions: immediate flushing of the channel with water, immediate flushing of the channel with 5% Triton X-100 (TX100) solution, and flushing of the channel after overnight soaking in PBS buffer. Immediate water flow led to very little recovery of the absorbed liposomes (Fig. 3e). Both PBS soaking and TX100 showed higher liposome recovery than water alone, with PBS soaking leading to 2 times more recovery than TX100. Porous silicon nanowires have previously been shown to degrade in the presence of PBS buffer,[24] and the by-product of the porous silicon degradation is low concentration silicic acid. The degradation of nanowire cilia loosens the trapping sites and allows for greater release of the

trapped liposomes, while leaving the vesicles intact, as opposed to TX100 that releases the trapped liposomes through vesicle rupture. Thus, dissolving the nanowires in PBS is an effective and non-destructive method for recovering any captured exosomes. The unmodified nanowires in PBS solution start to change in 4–6 h, and will degrade significantly in 24 h.[24] Our isolation experiment is typically done in 10 min, in which period the change of nanowire cilia is negligible. Hence, the ciliated structure is stable enough in the time scale of the isolation experiment.

## Conclusions

We have developed a fabrication protocol for novel ciliated micropillars, which are micropillars with porous silicon nanowires on the sidewalls, by integration of microfabrication, electroplating, and metal-assisted electroless nanowire etching. We fabricated a microfluidic prototype based on this hierarchical ciliated structure capable of the simultaneous multi-scale filtration of bio-fluids. We have demonstrated that the prototype can preferentially trap specifically sized liposomes within the high density of interstitial sites between the nanowires, while simultaneously filtering smaller proteins and larger particles with dimensions on the order of cellular debris. The trapped liposomes can then be released by dissolving the porous silicon nanowires in PBS buffer, allowing for the high purity recovery of intact liposomes. Further functionality should also be possible given the already established techniques for surface functionalizing porous silicon. Thus, this tunable hierarchical filtering technique offers the ability to rapidly, efficiently, and selectively enrich specific nanoscale components from complex biological samples, while maintaining their structural integrity, offering potential benefits to a range of both diagnostic and therapeutic applications.

## Acknowledgements

## Notes and references

1 B. Fevrier and G. Raposo, *Curr. Opin. Cell Biol.*, 2004, **16**, 415–421.

2 W. Stoorvogel, M. J. Kleijmeer, H. J. Geuze and G. Raposo, *Traffic*, 2002, **3**, 321–330.

3 C. Thery, L. Zitvogel and S. Amigorena, *Nat. Rev. Immunol.*, 2002, **2**, 569–579.

4 C. Lasser, V. S. Alikhani, K. Ekstrom, M. Eldh, P. T. Paredes, A. Bossios, M. Sjostrand, S. Gabrielsson, J. Lotvall and H. Valadi, *J. Transl. Med.*, 2011, **9**, 9.

5 A. V. Vlassov, S. Magdaleno, R. Setterquist and R. Conrad, *Biochim. Biophys. Acta, Gen. Subj.*, 2012, **1820**, 940–948.

6 K. Denzer, M. J. Kleijmeer, H. F. Heijnen, W. Stoorvogel and H. J. Geuze, *J. Cell Sci.*, 2000, **113**, 3365–3374.

7 C. Chen, J. Skog, C. H. Hsu, R. T. Lessard, L. Balaj, T. Wurdinger, B. S. Carter, X. O. Breakefield, M. Toner and D. Irimia, *Lab Chip*, 2010, **10**, 505–511.

8 X. Chen, Y. Ba, L. Ma, X. Cai, Y. Yin, K. Wang, J. Guo, Y. Zhang, J. Chen, X. Guo, Q. Li, X. Li, W. Wang, Y. Zhang, J. Wang, X. Jiang, Y. Xiang, C. Xu, P. Zheng, J. Zhang, R. Li, H. Zhang, X. Shang, T. Gong, G. Ning, J. Wang, K. Zen, J. Zhang and C.-Y. Zhang, *Cell Res.*, 2008, **18**, 997–1006.

9 E. Hosseini-Beheshti, S. Pham, H. Adomat, N. Li and E. S. Guns, *Mol. Cell. Proteomics*, 2012, **11**, 863–885.

10 H. Peinado, M. Aleckovic, S. Lavotshkin, I. Matei, B. Costa-Silva, G. Moreno-Bueno, M. Hergueta-Redondo, C. Williams, G. Garcia-Santos, C. M. Ghajar, A. Nitadori-Hoshino, C. Hoffman, K. Badal, B. A. Garcia, M. K. Callahan, J. Yuan, V. R. Martins, J. Skog, R. N. Kaplan, M. S. Brady, J. D. Wolchok, P. B. Chapman, Y. Kang, J. Bromberg and D. Lyden, *Nat. Med.*, 2012, **18**, 883–891.

11 J. L. Hood, S. San Roman and S. A. Wickline, *Cancer Res.*, 2011, **71**, 3792–3801.

12 C. Thery, M. Ostrowski and E. Segura, *Nat. Rev. Immunol.*, 2009, **9**, 581–593.

13 H. G. Zhang and W. E. Grizzle, *Clin. Cancer Res.*, 2011, **17**, 959–964.

14 A. Lakkaraju and E. Rodriguez-Boulan, *Trends Cell Biol.*, 2008, **18**, 199–209.

15 L. Alvarez-Erviti, Y. Seow, H. Yin, C. Betts, S. Lakhal and M. J. A. Wood, *Nat. Biotechnol.*, 2011, **29**, 341–345.

16 C. L. Mummery, R. P. Davis and J. E. Krieger, *Sci. Transl. Med.*, 2010, **2**, 27ps17.

17 R. C. Lai, F. Arslan, M. M. Lee, N. S. Sze, A. Choo, T. S. Chen, M. Salto-Tellez, L. Timmers, C. N. Lee, R. M. El Oakley, G. Pasterkamp, D. P. de Kleijn and S. K. Lim, *Stem Cell Res.*, 2010, **4**, 214–222.

18 R. C. Lai, T. S. Chen and S. K. Lim, *Regener. Med.*, 2011, **6**, 481–492.

19 J. M. Escola, M. J. Kleijmeer, W. Stoorvogel, J. M. Griffith, O. Yoshie and H. J. Geuze, *J. Biol. Chem.*, 1998, **273**, 20121–20127.

20 H. G. Lamparski, A. Metha-Damani, J.-Y. Yao, S. Patel, D.-H. Hsu, C. Ruegg and J.-B. Le Pecq, *J. Immunol. Methods*, 2002, **270**, 211–226.

21 A. Clayton, J. Court, H. Navabi, M. Adams, M. D. Mason, J. A. Hobot, G. R. Newman and B. Jasani, *J. Immunol. Methods*, 2001, **247**, 163–174.

22 B. J. Tauro, D. W. Greening, R. A. Mathias, H. Ji, S. Mathivanan, A. M. Scott and R. J. Simpson, *Methods*, 2012, **56**, 293–304.

23 D. D. Taylor, W. Zacharias and C. Gercel-Taylor, *Methods Mol. Biol.*, 2011, **728**, 235–246.

24 C. Chiappini, X. Liu, J. R. Fakhoury and M. Ferrari, *Adv. Funct. Mater.*, 2010, **20**, 2231–2239.

25 V. Lehmann and S. Ronnebeck, *J. Electrochem. Soc.*, 1999, **146**, 2968–2975.

26 M. S. Chandrasekar and M. Pushpavanam, *Electrochim. Acta*, 2008, **53**, 3313–3322.

27 H. Bohidar, *Colloid Polym. Sci.*, 1989, **267**, 292–300.